An inconspicuous, integrated electronic travel aid for visual impairment

Alain Boldini **Andy Louis Garcia** Marc Sorrentino *

Department of Mechanical and Aeronautical Engineering New York University Tandon School of Engineering Brooklyn, New York 11201

Mahya Beheshti Okpe Ogedegbe

Department of Rehabilitation Medicine New York University Langone Health Manhattan, New York 11201

Yi Fang

Department of Electrical and Computer Engineering Mechanical and Aeronautical Engineering New York University Tandon School of Engineering Brooklyn, New York 11201 Department of **Electrical and Computer Engineering** New York University Abu Dhabi Abu Dhabi (UAE)

Maurizio Porfiri †

Department of Department of Biomedical Engineering New York University Tandon School of Engineering Brooklyn, New York 11201

John-Ross Rizzo ‡

Department of Rehabilitation Medicine Department of Neurology New York University Langone Health Manhattan, New York 11201 Department of Biomedical Engineering New York University Tandon School of Engineering Brooklyn, New York 11201

With a globally aging population, visual impairment is an increasingly pressing problem for our society. This form of disability drastically reduces the quality of life and constitutes a large cost to the health care system. Mobility of the visually impaired is one of the most critical aspects affected by this disability, and yet it relies on low-tech solutions, such as the white cane and guide dogs. However, many avoid solutions entirely. In part, reluctance to use these solutions may be explained by their obtrusiveness, which is also a strong deterrent for the adoption of many new devices. In this paper, we leverage new advancements in artificial intelligence, sensor systems, and soft electroactive materials toward an electronic travel aid with an obstacle detection and avoidance system for the visually impaired. The travel aid incorporates a stereoscopic camera platform, enabling computer vision,

^{*}A. L. Garcia and M. Sorrentino contributed equally to this work.

[†]Corresponding author: mporfiri@nyu.edu.

[‡]Corresponding author: johnross.rizzo@nyulangone.org.

and a wearable haptic device that can stimulate discrete locations on the user's abdomen to signal the presence of surrounding obstacles. The proposed technology could be integrated into commercial backpacks and support belts, thereby guaranteeing a discreet and unobtrusive solution.

1 Introduction

Visual impairment is a continually growing problem, affecting over 3.2 million Americans who are 40 years and older [1]. This number is expected to double by 2050 [1], due to the aging population [2]. Visual impairment is associated with reduced quality of life [3], along with increased risk of falls and hip fractures [4], depression [5], obesity [6], and death [7]. Such a debilitating condition brings about high costs for society at large. A study on the impact of vision loss in Canada claimed that direct and indirect costs associated with visual impairment summed up to \$15.8 billion in 2007 (1.19% of the Country's gross domestic product), constituting the most expensive disease category in terms of health care expenditures [8].

Affording increased, safe mobility, and independence to the visually impaired is critical to improving their quality of life and reducing financial burden. Despite the severity of the situation at a global scale, options for enhancing the mobility of the visually impaired remain seldom employed, limited, and low-tech. To date, the most common options are white canes and guide dogs. Less than 10% [9, 10] of the visually impaired adopt these solutions, likely because of perceived social awkwardness, dependence, and anxiety [11–13]. These facts speak to the need for low-profile, inconspicuous assistive devices [14].

Technological advancements have the potential to provide alternative, cost-effective solutions for the immobility of the visually impaired. While regenerative medicine could ultimately restore vision [15], research in this area is still in its nascent stages and requires a bevy of therapeutic algorithms and alternatives for a comprehensive approach. Sensory substitution systems that amalgamate information and communication technology with artificial intelligence could enable localization, obstacle avoidance, and quality of life improvements in the short term [16]. However, most electronic travel aids (ETAs) proposed in the literature either enhance existing conspicuous solutions, such as smart white canes [17, 18], or develop bulky and obtrusive systems [19]. Overall, little to no attention has been paid toward the acceptance of these technologies by the visually impaired.

Here, we put forward a proof-of-concept ETA for the visually impaired that integrates a computer vision system for obstacle detection and a wearable device – a bookbag that seamlessly incorporates the sensors and a modified waist strap fashioned into a belt that provides haptic feedback to the user based on the computer vision output. The belt comprises a two-row, five-column array of piezoelectric-based tactors, which stimulate the abdomen based on the location of identified obstacles. More specifically, the computer vision software partitions the scene into an array of ten rectangular capture fields, resembling the tactors configuration on the torso;

if an obstacle is identified in one of these rectangles, the corresponding actuator in the array of tactors starts vibrating. The proposed solution allows for an inconspicuous, highly customizable design, which can be incorporated into commercial backpack systems.

Computer vision and generally deep learning have contributed significant advancements that can be integrated in assistive technologies for the visually impaired [20]. The use of a computer vision system supports the integration of critical features, such as object identification [21] or access to pedestrian signals [22]. The output from other types of sensors, such as ultrasonic or light detection and ranging (LIDAR) devices [23, 24], could also be integrated into our system through sensor fusion toward more accurate obstacle identification [21]. With respect to the wearable device, haptic feedback is preferred over auditory stimuli, since it provides faster information transfer for hazard negotiation, even if at a coarser level of detail [25]. A binaural bone conduction headset may also be wirelessly connected to the system through Bluetooth, enabling an additional communication channel.

The design proposed in this paper builds upon our previous belt prototype [26], which demonstrated the feasibility of relaying information through tactile feedback on the abdomen utilizing piezoelectric-based actuators. Compared to the previous device, the new prototype includes a higher spatial resolution with a larger number of tactors, along with improved vibration amplitude. In addition, our previous work did not include any sensing element, which is pursued herein through computer vision techniques.

In the following sections, we detail the design of the ETA. First, we describe the wearable haptic device and computer vision system. Then, we illustrate the interface between these components, and we perform a delay analysis. Finally, we describe potential areas of future research and experimental tests.

2 Wearable haptic device

The wearable haptic device consists of a belt with ten discrete tactors, capable of providing haptic feedback to the user. Similar to [26], actuation of the tactors is based on macrofiber composites (MFCs). Developed by NASA in 1999 [27], these materials are composed of piezoceramic wafers with interdigitated electrodes on a polyimide film, along with structural epoxy layers. We utilize P1-type MFC actuators from Smart Material (Sarasota, FL, United States). When a voltage on the order of kilovolts is applied across the electrodes, these MFCs elongate through the so-called d33 effect [28]. In other words, these materials exploit the non-zero coupling between the components of stress tensor and electric field in the poling direction [28].

The macroscopic deformations of MFCs are ultimately determined by boundary conditions. In our previous work [26], we exploited the nonlinear coupling between expansion and bending in a post-buckling configuration [29, 30]. To improve the performance of the actuator in terms of vibration amplitude and blocking force, we opt for an alternative solution, by gluing the MFC on a $54 \times 20 \times 0.25$ (length \times width

 \times thickness) mm aluminum plate using epoxy. In this configuration [31,32], the asymmetric elongation with respect to the neutral axis of the overall structure elicits out-of-plane bending.

To protect the actuator and prevent electric short circuits, we encapsulate the aluminum-backed MFC in a 3D-printed case made of polylactic acid (PLA), as shown in Fig. 1(a). Specifically, the actuator is fixed in a double cantilever configuration inside the case. Four 0.77 mm thick spacers are mounted between the actuator and the case to grant space for vibration. A hollow cylindrical protrusion is positioned anteriorly at the center of the actuator to transmit vibrations to the user's skin. The bottom part of the cylinder is 3D printed in thermoplastic polyurethane (TPU), and is connected to the case through two slender, flexible TPU rods. The top part of the cylinder, made of 3D-printed PLA, consists of a fixed cavity and a removable cap fitted through a threaded mechanism. The diameter of the area in contact with the abdomen is 14 mm. The internal cavity of the cylinder can accommodate additional masses to optimize the resonance frequency of the actuators.

Preliminary mechanical tests show that adding a mass of 12g reduces the resonance frequency to about 175 Hz [33], which is within the range of frequencies that skin mechanoreceptors are most sensitive to [25, 34]. These tests [33] also suggest that the peak-to-peak displacement of the tactors can be improved by a ten-fold factor throughout the frequency range of interest and more than a twenty-fold factor at resonance with respect to our previous design [26]. The resulting amplitude would be at least twice the sensory threshold over the entire actuation frequency range [25]. Further details about the design and characterization of the electromechanical properties of the actuators can be found in [33].

Tactors are arranged in five columns and two rows on a commercial hiking belt (Granite Gear, Two Harbors, MN, United States) that tethers to the backpack. More specifically, they are mounted on a thin aluminum beam-based scaffold, which is later applied to the belt, to maintain a minimum horizontal and vertical distance between the actuators of 130 and 110 mm, respectively. We expect this separation to improve users' discrimination performance, as previously demonstrated [25]. A custom-made tissue sleeve is wrapped around the belt to cover electrical connections and improve users' comfort, as shown in Fig. 1(b). Velcro® squares on the sleeve and tactors' cases ensure accurate positioning and prevent damping of the vibration from the sleeve.

MFC actuators are driven by an electrical circuit comprised of an Arduino Mega 2560 board (Arduino LLC, Boston, MA, United States), five printed circuit boards (PCBs), and five high-voltage amplifiers (HVAs). Each PCB connects to an HVA, which can simultaneously drive two actuators. PCBs integrate a dual-channel operational amplifier (TLC2202CP, Texas Instruments, Dallas, TX, United States) wired as an astable multivibrator. The switching frequency of the multivibrator is controlled by a dual-channel $10 \, \mathrm{k}\Omega$ digital potentiometer (AD8402ANZ10, Analog Devices Inc., Norwood, MA, United States), whose variable resistance is selected by the Arduino through a serial peripheral interface

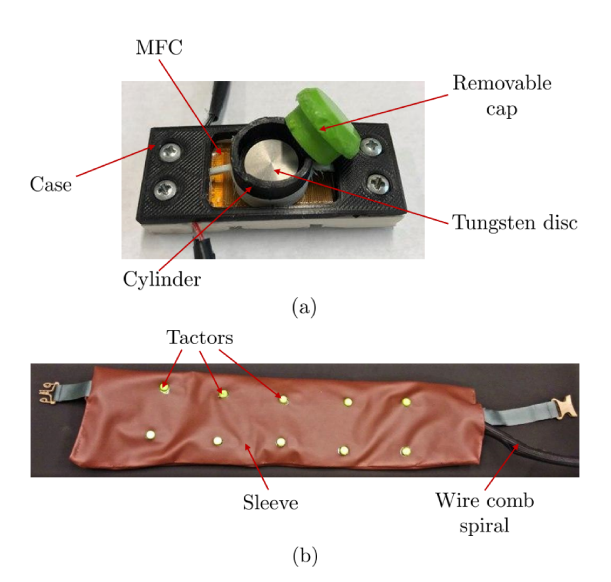


Fig. 1. (a) Tactor with open cap. The MFC is visible below the central cylinder, which contains a tungsten alloy $8\,\mathrm{g}$ disc. The wires coming out of the case are the MFC terminals. A detailed schematics of tactors can be found in [33]. (b) Assembled belt within a sleeve. The wires connecting the tactors to the electronics in the backpack are placed within the wire comb spiral visible on the right.

(SPI) protocol. The $0 \div 5\,\text{V}$ square wave generated by the multivibrator is fed to an HVA (AMT2012-CE3, Smart Material, Sarasota, FL, United States). The HVA maps linearly the $0 \div 2.5\,\text{V}$ range to $0 \div 0.5\,\text{kV}$, and the $2.5 \div 5\,\text{V}$ range to $0.5 \div 2\,\text{kV}$. The ground pin of the HVA provides a 500 V offset, such that the output voltage will be in the $-0.5 \div 1.5\,\text{kV}$ range.

Activation of PCBs and HVAs and modulation of the vibration frequency are achieved through a Matlab® R2019a script that controls the Arduino. PCB components are switched on by feeding a constant 5V signal to their power pins. HVAs are turned on by shorting their enabling pin. The vibration frequency is modulated by varying the resistance of the digital potentiometer between 0 and $10\,\mathrm{k}\Omega$, corresponding to $10\,\mathrm{Hz}$ and $390\,\mathrm{Hz}$, respectively, on 256 discrete levels. The desired level of resistance is selected by sending 10 bits through a SPI protocol. The Arduino board is controlled by a laptop through a USB 2.0 cord, which supplies the power for the PCBs.

Power for the HVAs is provided by a TalentCell 3 12V, 142.08 Wh lithium ion battery (PB120B1, TalentCell, Shenzen, Guangdong Province, China), weighing 1 kg. This battery allows an operational period of three hours, assuming that all the actuators are continuously vibrating at resonance. Connection between the lithium ion battery and HVAs is enabled by a break-out board through a standard 2.1 mm DC barrel-jack connector.

3 Computer vision system

The computer vision system utilizes a ZED stereo camera (Stereolabs Inc., San Francisco, CA, United States), which

enables reconstruction of the depth field from the acquired images. The camera is encapsulated in a custom-made 3D-printed case that is secured to the shoulder straps of the bookbag, and connected to a laptop through a USB 3.0 port.

We employ an Alienware 13 R3 (Dell, Round Rock, TX, United States) with an Ubuntu 16.04.6 LTS operating system as the main processing unit. Given the recent advancement in convolutional neural networks for object detection, in this paper we exploit such advances for real-time object detection. Our object detection method is adapted from the wellknown real-time object detection approach You Only Look Once (YOLO) [35] with Python 2.7 [36]. YOLO belongs to a family of computer vision algorithms that is currently able to identify over 9,000 classes of objects [37]. YOLO was selected due to its small elaboration time per image, which is critical for our application. YOLO was developed based on a single neural network applied to the full image; then, the image is divided into regions with different sizes, and finally bounding boxes and probabilities are predicted for each region. The system outputs 3D locations from the point cloud associated with each identified object, along with one of the originally implemented semantic labels [35] and its detection confidence. From these data, we compute the centroid of the object as the average of the location of its points. Further, we calculate the distance of the object as the Euclidean norm of the 3D vector at its centroid.

In order to spatiotopically map the obstacles to the tactors, we divide the acquired image in an array of ten equal rectangles, arranged in two rows and five columns, matching the spatial density of the belt. We assume that an object belongs to one of these rectangles when the projection of the centroid of the object on the image plane falls within the rectangle, see Fig. 2. This elaboration constitutes the activation signal for the tactors on the belt through the Arduino, as described in the next section. The algorithm can analyze images and provide these signals at a rate of 50 Hz, which is faster than the time in which typical saccadic eye movements would be able to acquire potential hazards [38].

4 Interface between the wearable haptic device and computer vision system

All the electronic components and the laptop are stored in a commercial backpack (V6012, Victoria Tourist, Amazon, Seattle, WA, United States), as shown in Fig. 3. The camera is mounted in front of the backpack, in order to maintain alignment with the torso and avoid possible confounds due to head motion; the torso is never misaligned with the intended travel path whereas the head and other potential body areas/segments often are. The tactors are connected to the HVAs in the backpack through channeled wires, which are covered by the sleeve and by a binding coil, as shown in Fig. 1(b).

The electronics of the haptic device is interfaced with the computer vision system through the main processing unit, as shown in Fig. 4. More specifically, we utilize a transmission control protocol (TCP) to establish a connection between the computer vision algorithm in Python 2.7 and the

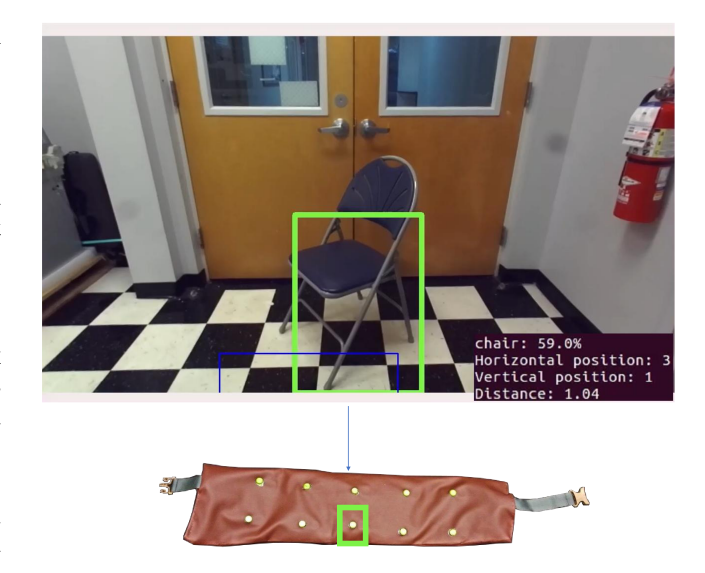


Fig. 2. Example of the elaboration from the computer vision system. In the image acquired by the camera, a chair is identified with 59.0% confidence in the third column from the left and first row from the bottom, at a distance of $1.04\,\mathrm{m}$ from the camera (see bottom right of the computer vision image). The corresponding actuator (here in a green frame) in a spatiotopically preserved manner will vibrate on the belt to signal the presence of the obstacle.

Arduino control script in Matlab® R2019b. When the system is turned on, as a first step, the Matlab script initializes the Arduino and opens the TCP, functioning as a server. Next, the Python code establishes the connection as client and begins to acquire images from the ZED camera, while the Matlab script enters a spinning loop, waiting for data from the computer vision system. Once a frame is acquired, it is analyzed by the Python code, which identifies all the objects present in the scene. For each object that is detected, the Python code sends two numbers to the Matlab script: the identifier number of the tactor to switch on, and the distance of the object. Finally, the Matlab script processes the received information, sends signals to the Arduino, and re-enters the spinning loop. To avoid saturating the connection and to limit power consumption, delays of 30 ms and 25 ms are added after each information transfer in Python and after each check during the spinning loop in Matlab, respectively.

Matlab reads all the information in the TCP queue. For each detected object, it first verifies the depth of the object from the end user and then maps the distance to a frequency, such that closer objects will have a higher frequency, with the closest objects at the resonance frequency. To facilitate frequency discrimination, we consider only discrete frequency steps.

Specifically, we set the frequency to a level in the $25 \div 175\,\text{Hz}$ range, with intervals of approximately 25 Hz. First, a peri-personal distance range, $1 \div 10\,\text{m}$ is mapped linearly to the $10 \div 175\,\text{Hz}$ frequency range, with $10\,\text{m}$ mapped to $10\,\text{Hz}$ and $1\,\text{m}$ mapped to $175\,\text{Hz}$. Then, we round the obtained frequency to the closest admissible integer frequency. The frequency is then mapped to a resistance value, which is sent to



Fig. 3. Overall system on a person. The belt, here exposed for the sake of clarity, can be worn below personal garments. The camera, fixed on one of the two backpack straps, is locked in position with a buckle after the backpack is worn.

the digital potentiometer on the PCBs through SPI protocol. If the corresponding tactor is already on, no further action is taken, otherwise, it is switched on for 200ms. Such an intermittent pulse allows for easier vibration discrimination, as compared to continuous stimulation, which would elicit habituation.

To assess performance of the connection between the computer vision system and the haptic device, we performed two experiments, through which we sought to quantify the elaboration and transmission delay in the Python and Matlab codes, respectively. These two tests were performed independently to minimize the delay associated to saving the results. During the two experiments, the experimenter carried the computer vision system connected to the Arduino in the backpack to analyze an environment; the participant walked in a repeated back-and-forth cycle along a corridor of length of about 5 m. During ambulation, the ZED camera scanned the ambient space. The obstacles, encompassing a desk, multiple chairs, computers, monitors, laptops, and other smaller objects, were at fixed and known locations. Since our experiments focus on the interface between the computer vision system and the wearable haptic device, we do not consider performance of the individual subsystems (such as accuracy in object classification or vibration intensity).

More specifically, in the first experiment, we run the computer vision code in Python for about three minutes while



Fig. 4. Schematics of the integrated ETA proposed in this paper. The ZED camera acquires images, which are analyzed by the Python 2.7 computer vision code running on the Alienware laptop. The output of the Python code is sent through a TCP connection to a Matlab script that controls the Arduino. The Arduino drives five dual-channel PCBs, each connected to a dual-channel HVA. Each HVA controls a column of two actuators on the belt.

measuring the time elapsed from image acquisition to transmission of data to the Matlab script, along with the number of identified objects. We exclude from our analysis all the acquired frames in which no object was detected by the computer vision system. For each frame that contain at least one identified object, we consider three contributions of the delay in the Python script: the time to acquire the image and identify all point clouds in the frame ("PtCl"), to classify the detected objects and compute their distances ("Clas"), and to determine the position of the centroid of each object in the image and send all data through the TCP connection ("Send"). We consolidate all these contributions in the total delay in the Python code ("Tot").

In Fig. 5, we show boxplots indicating the delay for each of these operations. The median value of the total delay is 20.9 ms. Identifying the position of the objects and sending the data through the TCP have a negligible contribution to this delay, which is mostly determined by the operations in YOLO (generating the point cloud and labelling the objects, PtCl and Clas). We observe that the distributions of delays are skewed, with most of the data around the median value

and a significant tail toward larger delays. Thus, the system normally behaves as expected, but in several instances the delays increase significantly. Interestingly, the Pearson correlation coefficient indicates that only the time to send data through TCP correlates with the number of detected objects in the frame (r=0.93), whereas all the other contributions and the total delay do not (r<0.22). Thus, the performance of the Python script is independent of the number of objects detected in the frames.

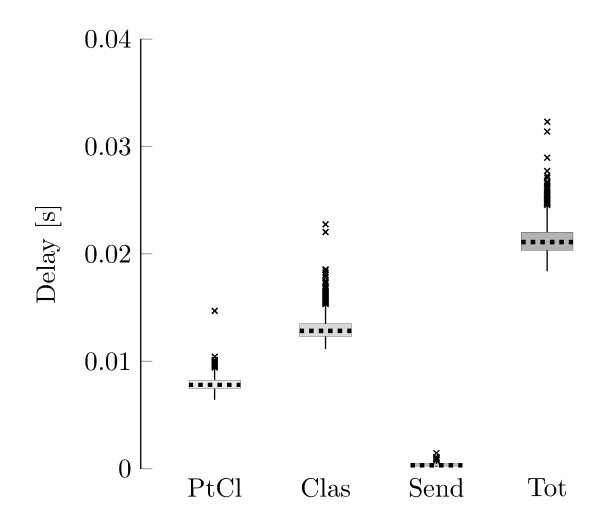


Fig. 5. Contributions to the delay in the Python script, over 4745 object detections in 2662 frames, over a total of 3918 acquired frames. "PtCl" is the time required to reconstruct the point cloud of all the objects in the frame, "Clas" represents the time to assign a label to each object and determine its distance, and "Send" indicates the time required for determining the position of all the objects in the frame and sending all data through the TCP connection. "Tot" is the total delay, computed by summing all the previous contributions. Dash lines are the medians, boxes delimit the first and third quartiles, vertical lines indicate the 1.5-interquartile range, and crosses are outliers.

In the second experiment, we systematically investigate the delay in the Matlab script. Similar to the previous case, we run for about five minutes the computer vision code in Python, which transmits data through TCP to the Matlab script that elaborates and sends data downstream to Arduino. In this case, we consider each reading of the TCP queue, which may contain multiple objects from several frames. We consider four contributions to the transmission delay in Matlab: the time to receive the data from the TCP ("Read"), to elaborate on the numbers to find the corresponding pins and the resistance value for the potentiometer ("Elab"), to send data through the SPI protocol and modify the potentiometer resistance toward changing the vibration frequency ("Freq"), and to turn on electronic components of the PCBs, activate the corresponding actuators by shorting the enable pin of the HVAs, and provide the input voltages to the operational amplifiers ("On"). Further, we calculate the total time ("Tot") to obtain the data from the Python code and send it to the Arduino as the sum of the previous contributions. In addition,

we record the number of objects in the TCP queue.

The results of this delay analysis are shown in Fig. 6. The median value of the total delay is 80.6 ms, with the largest contributions due to the operations of the Arduino to modify the vibration frequency or activate the electronics. This value corresponds to a median time from acquisition to stimulation of 101.5 ms, that is, an effective frequency of almost 10 Hz. Similar to the previous case, the dispersion of the data regarding the delay contributions in the Matlab script is significant, with a non-Gaussian distribution skewed toward lower values. Large delays may be related to freezing of the SPI connection, which causes the Arduino to reset. By computing the Pearson correlation coefficient, we find that delays are not correlated to the number of objects in the TCP queue (|r| < 0.04 for all contributions and total time). The significant delay introduced by Arduino calls for the adoption of a more robust and reliable way to interface with the electronics. Despite the delay, given that the number of detected objects in the TCP queue does not keep increasing, we expect that the Matlab script should be able to keep up with the transmission, emptying the queue accumulating in the TCP connection. This claim requires further integrated analyses during longer utilization periods, which will indicate the actual transmission delay between image acquisition and tactor activation.

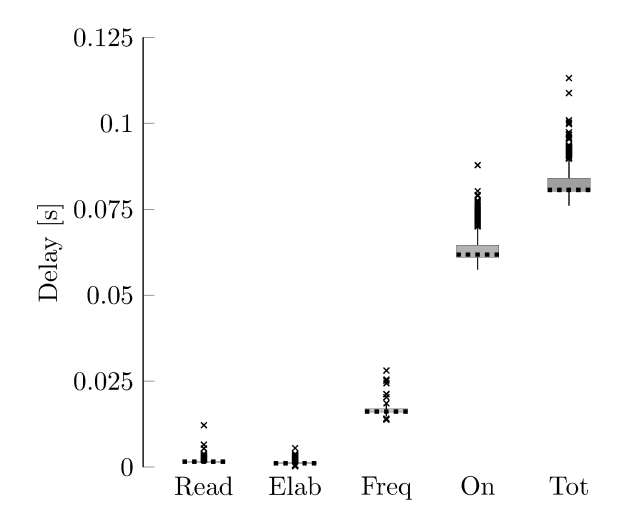


Fig. 6. Contributions to the delay in the Matlab script, over 9209 object detections, in 2942 TCP queue readings. "Read" indicates the reading from the TCP connection, "Elab" is the elaboration time of acquired data, "Freq" represents the time required to change the actuation frequency, "On" is the time to turn on the electronics, short the enable pin of the HVAs, and start generating the square-wave. "Tot" is the total delay, computed by summing all the previous contributions. Dash lines are the medians, boxes delimit the first and third quartiles, vertical lines indicate the 1.5-interquartile range, and crosses are outliers.

5 Conclusions

In this work, we developed a new, integrated ETA for visual impairment. The ETA comprises a computer vision system for obstacle detection and a bookbag-based belt with discrete tactors, providing haptic feedback relative to obstacle location in an egocentric, spatiotopically preserved reference frame. Compared to solutions proposed in the literature, our system constitutes a customizable, inconspicuous option, whereby the belt could be detached and worn under personal garments and the remaining electronics and sensing components could be integrated in commercial backpacks. This ETA and approaches fashioned in a similar way could address the needs of the visually impaired, delivering unobtrusive aesthetics and an ergonomic design, critical aspects for the adoption of new assistive technologies [13, 14].

Future studies and improvements are necessary to ensure usability of the device and potential commercialization. While preliminary mechanical tests were performed on the tactors, systematic, rigorous testing is required to quantify their performance against the previous generation of actuators [26]. In this vein, discrimination tests [25] will provide a first benchmark to assess the capabilities of our new wearable device. When testing the performance of the integrated system, we expect that our current control system will not relay information to the user with high fidelity in all circumstances. For example, it is untenable to assume that the vibration of multiple actuators in the presence of multiple obstacles will provide meaningful data to the end user, rather it is likely to create sensory overload; this must be addressed through adaptive vibratory and/or audio messages. These observations warrant further investigation toward the development of a more sophisticated control system. After optimizing the control system, we will test the performance of our device against analogous systems in the literature. Finally, several technical aspects, including miniaturization of the main processing unit, a single integrated software script for both computer vision and control of the belt's microprocessor, and incorporation of the tactors into customized backpack waiststraps, should be considered toward a wearable device with significant commercial appeal.

Acknowledgements

This research was supported by Connect-the-Dots Pilot Award (New York University Langone Health and Tandon School of Engineering) and by the National Science Foundation under Grant No. CMMI-1433670.

6 Competing interests

Dr. Rizzo discloses conflictual interests as a result of intellectual property owned by New York University and related advisory positions with equity and ad hoc compensation. In the future, the aforementioned project may relate to multicomponent wearable technologies relevant to the stated interests.

References

- [1] Varma, R., Vajaranant, T. S., Burkemper, B., Wu, S., Torres, M., Hsu, C., Choudhury, F., and McKean-Cowdin, R., 2016. "Visual impairment and blindness in adults in the United States: Demographic and geographic variations from 2015 to 2050". *JAMA ophthalmology*, 134(7), pp. 802–809.
- [2] Stevens, G. A., White, R. A., Flaxman, S. R., Price, H., Jonas, J. B., Keeffe, J., Leasher, J., Naidoo, K., Pesudovs, K., Resnikoff, S., Taylor, H., and Bourne, R. R., 2013. "Global prevalence of vision impairment and blindness: Magnitude and temporal trends, 1990–2010". Ophthalmology, 120(12), pp. 2377–2384.
- [3] Sherwood, M. B., Garcia-Siekavizza, A., Meltzer, M. I., Hebert, A., Burns, A. F., and McGorray, S., 1998. "Glaucoma's impact on quality of life and its relation to clinical indicators: a pilot study". *Ophthalmology*, 105(3), pp. 561–566.
- [4] Legood, R., Scuffham, P., and Cryer, C., 2002. "Are we blind to injuries in the visually impaired? A review of the literature". *Injury Prevention*, **8**(2), pp. 155–160.
- [5] Zhang, X., Bullard, K. M., Cotch, M. F., Wilson, M. R., Rovner, B. W., McGwin, G., Owsley, C., Barker, L., Crews, J. E., and Saaddine, J. B., 2013. "Association between depression and functional vision loss in persons 20 years of age or older in the United States, NHANES 2005–2008". JAMA Ophthalmology, 131(5), pp. 573– 581.
- [6] Seddon, J. M., Cote, J., Davis, N., and Rosner, B., 2003. "Progression of age-related macular degeneration: Association with body mass index, waist circumference, and waist-hip ratio". Archives of Ophthalmology, 121(6), pp. 785–792.
- [7] McCarty, C. A., Nanjan, M. B., and Taylor, H. R., 2001. "Vision impairment predicts 5 year mortality". *British Journal of Ophthalmology*, **85**(3), pp. 322–326.
- [8] Access Economics Pty Limited, 2009. The cost of vision loss in Canada. Summary report. Tech. rep., CNIB and the Canadian Ophthalmological Society.
- [9] Winter, B. 10 fascinating facts about the white cane. https://www.perkins.org/stories/10-fascinatingfacts-about-the-white -cane. Perkins School for the Blind, Accessed: 2020-02-16.
- [10] How many people use Guide Dogs? https://www.guidingeyes.org/about/faqs/. Guiding Eyes for the Blind, Accessed: 2020-02-16.
- [11] Rogers, P. The white cane: Symbol of dependence or independence. https://www.visionaware.org/blog/visually-impaired-now-what/the-white-cane-symbol-of-dependence-or-independence/12. VisionAwareTM, Accessed: 2020-02-16.
- [12] What will people think about me if i use a white cane? https://www.visionaware.org/info/everyday-living/essential-skills/an-introduction-to-orientation-and
 - -mobility-skills/what-will-people

- -think-about-me-if-i-use-a-white-cane/1235. VisionAwareTM, Accessed: 2020-02-16.
- [13] Ye, H., Malu, M., Oh, U., and Findlater, L., 2014. "Current and future mobile and wearable device use by people with visual impairments". In Proceedings of the SIGCHI Conference on Human Factors in Computing Systems, pp. 3123–3132.
- [14] Shinohara, K., and Wobbrock, J. O., 2011. "In the shadow of misperception: Assistive technology use and social interactions". In Proceedings of the SIGCHI Conference on Human Factors in Computing Systems, pp. 705–714.
- [15] Stern, J. H., Tian, Y., Funderburgh, J., Pellegrini, G., Zhang, K., Goldberg, J. L., Ali, R. R., Young, M., Xie, Y., and Temple, S., 2018. "Regenerating eye tissues to preserve and restore vision". *Cell Stem Cell*, 22(6), pp. 834–849.
- [16] Pissaloux, E., and Velazquez, R., 2017. *Mobility of visually impaired people. Fundamentals and ICT assistive technologies*. Springer.
- [17] Rizzo, J.-R., Conti, K., Thomas, T., Hudson, T. E., Wall Emerson, R., and Kim, D. S., 2018. "A new primary mobility tool for the visually impaired: A white cane—adaptive mobility device hybrid". Assistive Technology, 30(5), pp. 219–225.
- [18] Ulrich, I., and Borenstein, J., 2001. "The GuideCane Applying mobile robot technologies to assist the visually impaired". *IEEE Transactions on Systems, Man, and Cybernetics-Part A: Systems and Humans,* 31(2), pp. 131–136.
- [19] Dakopoulos, D., and Bourbakis, N. G., 2009. "Wearable obstacle avoidance electronic travel aids for blind: a survey". *IEEE Transactions on Systems, Man, and Cybernetics, Part C (Applications and Reviews),* **40**(1), pp. 25–35.
- [20] Bhowmick, A., and Hazarika, S. M., 2017. "An insight into assistive technology for the visually impaired and blind people: state-of-the-art and future trends". *Journal on Multimodal User Interfaces*, **11**(2), pp. 149–172.
- [21] Rizzo, J.-R., Pan, Y., Hudson, T., Wong, E. K., and Fang, Y., 2017. "Sensor fusion for ecologically valid obstacle identification: Building a comprehensive assistive technology platform for the visually impaired". In 2017 7th International Conference on Modeling, Simulation, and Applied Optimization (ICMSAO), IEEE, pp. 1–5.
- [22] Li, X., Cui, H., Rizzo, J.-R., Wong, E., and Fang, Y., 2019. "Cross-Safe: A computer vision-based approach to make all intersection-related pedestrian signals accessible for the visually impaired". In Science and Information Conference, Springer, pp. 132–146.
- [23] Bhatlawande, S. S., Mukhopadhyay, J., and Mahadevappa, M., 2012. "Ultrasonic spectacles and waist-belt for visually impaired and blind person". In 2012 National Conference on Communications (NCC), IEEE, pp. 1–4.
- [24] Ton, C., Omar, A., Szedenko, V., Tran, V. H., Aftab, A., Perla, F., Bernstein, M. J., and Yang, Y., 2018. "Lidar assist spatial sensing for the visually impaired and perfor-

- mance analysis". *IEEE Transactions on Neural Systems and Rehabilitation Engineering*, **26**(9), pp. 1727–1734.
- [25] Cholewiak, R. W., Brill, J. C., and Schwab, A., 2004. "Vibrotactile localization on the abdomen: Effects of place and space". *Perception & Psychophysics*, **66**(6), pp. 970–987.
- [26] Phamduy, P., Rizzo, J.-R., Hudson, T. E., Torre, M., Levon, K., and Porfiri, M., 2018. "Communicating through touch: Macro fiber composites for tactile stimulation on the abdomen". *IEEE Transactions on Haptics*, **11**(2), pp. 174–184.
- [27] Wilkie, W. K., Bryant, R. G., High, J. W., Fox, R. L., Hellbaum, R. F., Jalink Jr, A., Little, B. D., and Mirick, P. H., 2000. "Low-cost piezocomposite actuator for structural control applications". In Proceedings of SPIE 3991, Smart Structures and Materials 2000: Industrial and Commercial Applications of Smart Structures Technologies, Vol. 3991, pp. 323–334.
- [28] Tiersten, H. F., 2013. Linear piezoelectric plate vibrations: Elements of the linear theory of piezoelectricity and the vibrations piezoelectric plates. Springer.
- [29] Humer, A., 2013. "Exact solutions for the buckling and postbuckling of shear-deformable beams". *Acta Mechanica*, **224**(7), pp. 1493–1525.
- [30] Neukirch, S., Frelat, J., Goriely, A., and Maurini, C., 2012. "Vibrations of post-buckled rods: the singular inextensible limit". *Journal of Sound and Vibration*, **331**(3), pp. 704–720.
- [31] Erturk, A., and Delporte, G., 2011. "Underwater thrust and power generation using flexible piezoelectric composites: An experimental investigation toward self-powered swimmer-sensor platforms". *Smart Materials and Structures*, **20**(12), p. 125013.
- [32] Cha, Y., Chae, W., Kim, H., Walcott, H., Peterson, S. D., and Porfiri, M., 2016. "Energy harvesting from a piezo-electric biomimetic fish tail". *Renewable Energy*, **86**, pp. 449–458.
- [33] Boldini, A., Rizzo, J.-R., and Porfiri, M., 2020. "A piezoelectric-based advanced wearable: obstacle avoidance for the visually impaired built into a backpack". In Nano-, Bio-, Info-Tech Sensors, and 3D Systems IV, Vol. 11378, International Society for Optics and Photonics, p. 1137806.
- [34] Bolanowski Jr, S. J., Gescheider, G. A., Verrillo, R. T., and Checkosky, C. M., 1988. "Four channels mediate the mechanical aspects of touch". *The Journal of the Acoustical Society of America*, **84**(5), pp. 1680–1694.
- [35] Redmon, J., Divvala, S., Girshick, R., and Farhadi, A., 2016. "You only look once: Unified, real-time object detection". In Proceedings of the IEEE conference on computer vision and pattern recognition, pp. 779–788.
- [36] 3D Object detection using Yolo and the ZED in Python and C++. https://github.com/stereolabs/zed-yolo. StereoLabs - GitHubTM, Accessed: 2020-02-16.
- [37] Redmon, J., and Farhadi, A., 2017. "Yolo9000: Better, faster, stronger". In Proceedings of the IEEE Conference on Computer Vision and Pattern Recognition, pp. 7263–7271.

[38] Leigh, R. J., and Zee, D. S., 2015. *The neurology of eye movements*. Oxford University Press.